J|A|C|S ARTICLES

Published on Web 01/30/2009

Design of SERS-Encoded, Submicron, Hollow Particles Through Confined Growth of Encapsulated Metal Nanoparticles

Marcos Sanles-Sobrido, Wibke Exner, Laura Rodríguez-Lorenzo, Benito Rodríguez-González, Miguel A. Correa-Duarte,* Ramon A. Álvarez-Puebla,* and Luis M. Liz-Marzán

Departamento de Química Física and Unidad Asociada CSIC, Universidade de Vigo, 36310 Vigo, Spain

Received November 11, 2008; E-mail: macorrea@uvigo.es; ramon.alvarez@uvigo.es

Abstract: The synthetic architectures of complex inorganic nanostructures, including multifunctional hollow capsules, are expected to play key roles in many different applications, such as drug delivery, photonic crystals, nanoreactors, and sensing. Implementation of novel strategies for the fabrication of such materials is needed because of the infancy of this knowledge, which still limits progress in certain areas. Herein we report a straightforward synthetic approach for the development of multifunctional submicron reactors comprising catalytic gold nanoparticles (2−3 nm) confined inside hollow silica capsules. Additionally, the confined growth of encapsulated metal nanoparticles was carried out to evidence the usefulness and functionality of these reactors in catalytic applications and as an approach for the development of novel complex nanostructures. Their potential and multifunctionality have been pointed out by fabrication of SERS-encoded submicrometer particles with shape and size uniformity for use in antigen biosensing; this was accomplished via codification of gold nanoparticle islands grown onto their inner surfaces.

Introduction

Precise diagnosis and proper therapeutic treatments for preventing and controlling pandemics and other biothreads are central to human health. Most of the established strategies for detection assays rely on specific receptor−ligand molecular recognition (for example, antibody−antigen or complementary oligonucleotide). In line with this, encoded supports are simple, cost-effective platforms amenable to multiplexing and high-throughput screening assays.[1−7] Several strategies have been developed for the preparation of encoded particles,[8−10] among which those based on vibrational spectroscopy[11] present advantages related to unambiguous classification of the encoded particles and the availability of thousands of different barcodes. Although Raman and IR spectroscopies are reliable, enhancement of the barcoded vibrational signal is required to improve the detection speed and sensitivity as well as to decrease the encoded particle size. In this context, surface-enhanced Raman scattering (SERS) spectroscopy offers a unique solution for amplification of the vibrational signal[12] along with decreases in both read-out time and particle size. For SERS to be achieved, close contact between the molecular probe and the optical enhancer (typically silver or gold nanostructures) is necessary. Several synthetic strategies for the fabrication of micron-sized metal nanoparticle (MNP)-based composite beads have been developed, including chemisorption,[13] physisorption,[14] emulsion polymerization,[15] electron-beam evaporation[16] and the versatile layer-by-layer (LbL) assembly technique.[17,18] These approaches were aimed at controlling the nanocomposite's optical and

(1) Braeckmans, K.; De Smedt, S. C.; Leblans, M.; Roelant, C.; Demeester, J. *Nat. Rev. Drug Discovery* **2002**, *1*, 1–10.
(2) Fenniri, H.; Alvarez-Puebla, R. *Nature Chem. Biol.* **2007**, *3*, 247–249.
(3) Bake, K. D.; Walt, D. R. *Annu. Rev. Anal. Chem.* **2008**, *1*, 515–547.
(4) Doering, W. E.; Piotti, M. E.; Natan, M. J.; Freeman, R. G. *Adv. Mater.* **2007**, *19*, 3100–3108.
(5) Freeman, R. G.; Raju, P. A.; Norton, S. M.; Walton, I. D.; Smith, P. C.; He, L.; Natan, M. J.; Sha, M. Y.; Penn, S. G. *Methods Mol. Biol. (Totowa, NJ)* **2005**, *303*, 73–83.
(6) Nicewarner-Peña, S. R.; Freeman, R. G.; Reiss, B. D.; He, L.; Peña, D. J.; Walton, I. D.; Cromer, R.; Keating, C. D.; Natan, M. J. *Science* **2001**, *294*, 137–141.
(7) Sha, M. Y.; Walton, I. D.; Norton, S. M.; Taylor, M.; Yamanaka, M.; Natan, M. J.; Xu, C.; Drmanac, S.; Huang, S.; Borcherding, A.; Drmanac, R.; Penn, S. G. *Anal. Bioanal. Chem.* **2006**, *384*, 658–666.
(8) Cunin, F.; Schmedake, T. A.; Link, J. R.; Li, Y. Y.; Koh, J.; Bhatia, S. N.; Sailor, M. J. *Nat. Mater.* **2002**, *1*, 39–41.
(9) Finkel, N. H.; Lou, X.; Wang, C.; He, L. *Anal. Chem.* **2004**, *76*, 353A–359A.
(10) Pregibon, D. C.; Toner, M.; Doyle, P. S. *Science* **2007**, *315*, 1393–1396.
(11) Raez, J.; Blais, D. R.; Alvarez-Puebla, R. A.; Bravo-Vasquez, J. P.; Pezacki, J. P.; Fenniri, H. *Langmuir* **2007**, *23*, 6482–6485.
(12) Aroca, R. F. *Surface-Enhanced Vibrational Spectroscopy*; Wiley: New York, 2006.
(13) Li, G.; Fan, J.; Jiang, R.; Gao, Y. *Chem. Mater.* **2004**, *16*, 1835–1837.
(14) Zhang, J.; Xu, S.; Kumacheva, E. *J. Am. Chem. Soc.* **2004**, *126*, 7908–7914.
(15) Quaroni, L.; Chumanov, G. *J. Am. Chem. Soc.* **1999**, *121*, 10642–10643.
(16) Correa-Duarte, M. A.; Salgueirino-Maceira, V.; Rodriguez-Gonzalez, B.; Liz-Marzan, L. M.; Kosiorek, A.; Kandulski, W.; Giersig, M. *Adv. Mater.* **2005**, *17*, 2014–2018.
(17) Caruso, F.; Spasova, M.; Salgueirino-Maceira, V.; Liz-Marzan, L. M. *Adv. Mater.* **2001**, *13*, 1090–1094.
(18) Lou, X. W.; Yuan, C.; Rhoades, E.; Zhang, Q.; Archer, L. A. *Adv. Funct. Mater.* **2006**, *16*, 1679–1684.

Scheme 1. Schematic Illustrations of the Multistep (a) Fabrication and (b) Codification, Biofunctionalization, and Biosensing Procedures[a] and of (c) the Biosensing Assay[b]

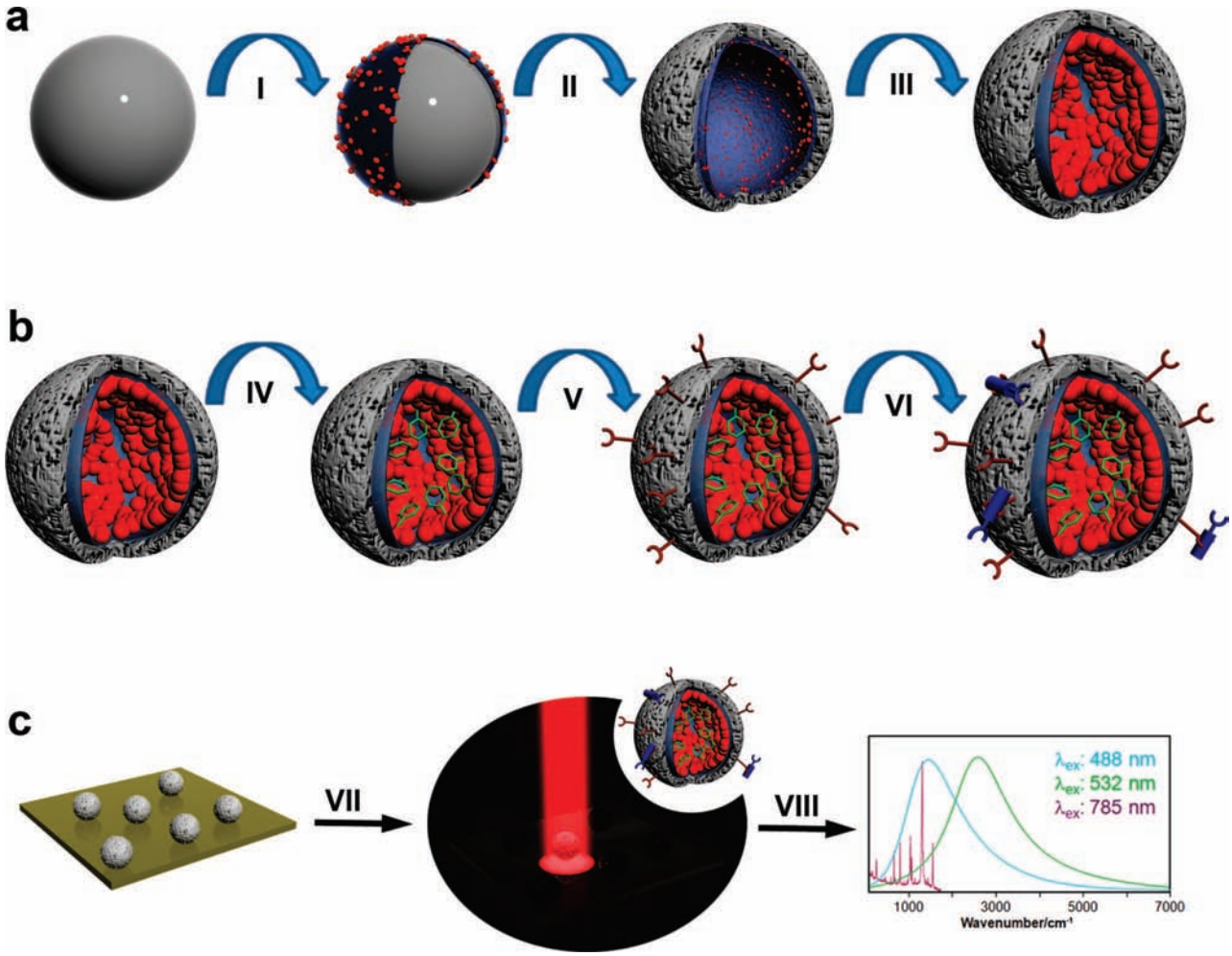

[a] (I) Polyelectrolyte coating of PS beads and Au seed deposition; (II) PVP wrapping, silica coating, and PS dissolution; (III) seeded Au NP growth; (IV) SERS probe diffusion; (V) antibody attachment; (VI) antigen biorecognition. [b] (VII) Illumination of the capsule mixture with different laser lines; (VIII) spectral deconvolution.

chemical properties as well as exploring different product end uses in sensor design,[19] catalysis,[20] and spectroscopic labeling.[21] However, MNPs produced by most of the currently available synthetic methods are located on the outer surface of the microparticle, which encompasses several problems, such as (a) a low MNP/supporting-material ratio; (b) possible side reactions due to the catalytic activity of the MNPs; (c) signal enhancement of the given analyte that overlaps the microparticle barcode; (d) difficult functionalization of the particle surface for the immobilization of biomolecules; and (e) leaching out of the vibrational label, thus decreasing the particle signal and promoting toxic reactions.

To circumvent all of these drawbacks, we have designed useful submicron-sized reactors composed of hollow silica capsules with a high density of metallic nanoparticles decorating their inner surfaces. A few examples of the use of active nanoparticles inside nano- and submicroreactors for the design of complex inorganic nanostructures have been reported.[22,23] In particular, these heterostructures were demonstrated to have great potential because of the catalytic activity of the metallic nanoparticles. On the basis of the great potential of such reactors, we report in this work the development of a novel, specific, and robust synthetic strategy for the preparation of SERS-encoded submicrometer particles with shape and size uniformity; this approach is based on the generation and codification of gold nanoparticles on the inner surfaces of monodisperse, hollow silica capsules. The size of the resulting capsules is optimized to be small enough to maintain colloidal stability while carrying antibodies yet big enough for a single particle to be readily resolved by conventional confocal Raman microspectroscopy. Proof of concept for biosensing applications of this material and its potential multiplexing capabilities are additionally demonstrated.

Scheme 1a shows the overall procedure for the fabrication, codification, biofunctionalization, and biosensing proof of concept of the SERS-encoded silica capsules. Detailed procedures are described in the Experimental Section; briefly,

(19) Shenhar, R.; Rotello, V. M. *Acc. Chem. Res.* **2003**, *36*, 549–561.
(20) Vriezema, D. M.; Comellas-Aragones, M.; Elemans, J. A. A. W.; Cornelissen, J. J. L. M.; Rowan, A. E.; Nolte, R. J. M. *Chem. Rev.* **2005**, *105*, 1445–1490.
(21) Thomas, K. G.; Kamat, P. V. *Acc. Chem. Res.* **2003**, *36*, 888–898.
(22) Yin, Y.; Rioux, R. M.; Erdonmez, C. K.; Hughes, S.; Somorjai, G. A.; Alivisatos, A. P. *Science* **2004**, *304*, 711–714.
(23) Lee, J.; Park, J. C.; Song, H. *Adv. Mater.* **2008**, *20*, 1523–1528.

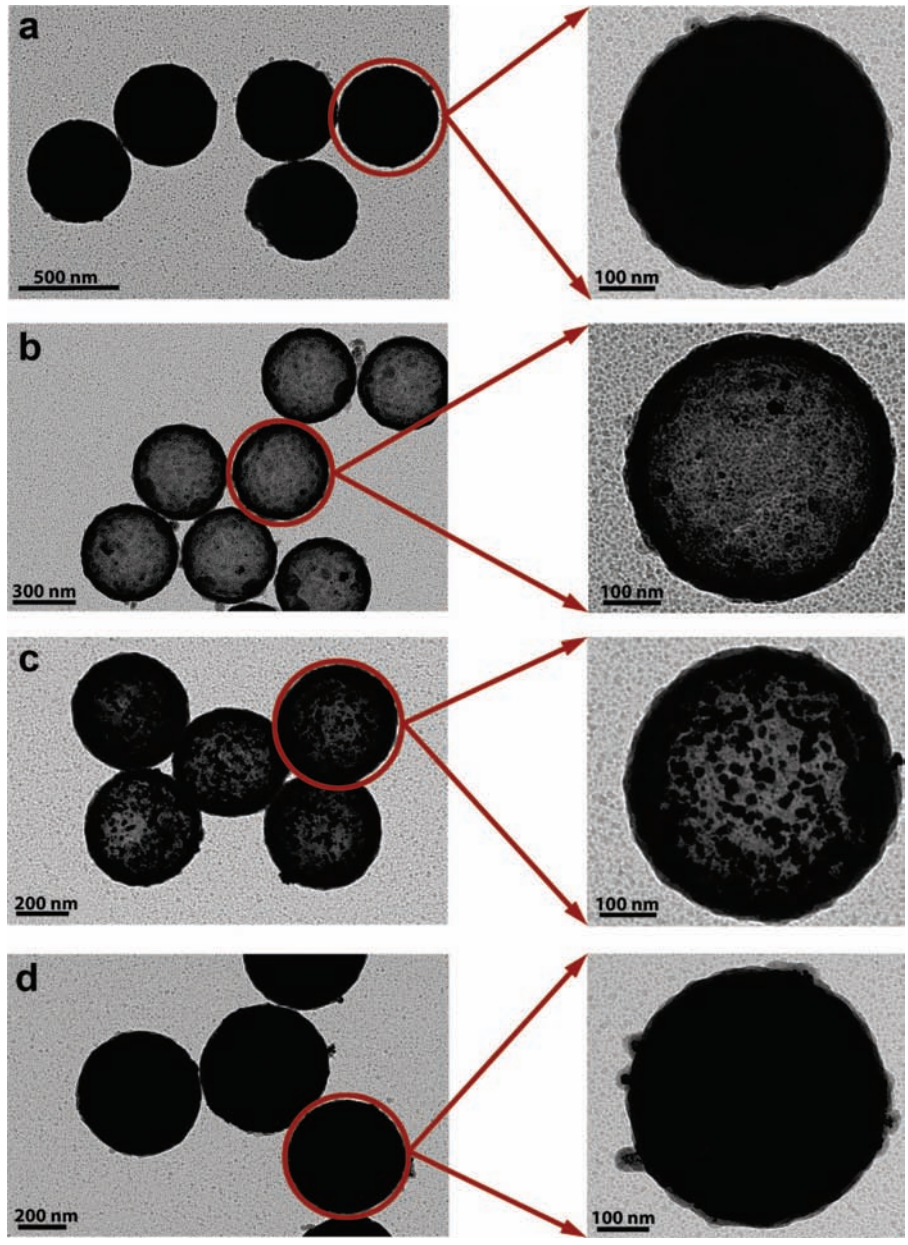

Figure 1. (left) Low- and (right) high-magnification TEM micrographs of spherical particles at various stages of fabrication: (a) PS@Au-seeds@SiO_2; (b) Au-seeds@SiO_2-h; (c) Au-NPs@SiO_2-h; and (d) Au-GNPs@SiO_2-h.

homogeneous 530 nm polystyrene (PS) beads were coated with four alternating polyelectrolyte monolayers using the electrostatic self-assembly LbL protocol.[24] Four layers of polymer, rather than just two, were deposited in order to improve the homogeneity of the coating shell and generate the positive surface charge [ζ potential (ζ) = +40 mV] necessary for the electrostatic adsorption of 1−3 nm gold seeds (ζ = −20 mV), yielding PS@Au-seeds [Scheme 1a, step I; see Figure S1a−c[25] for transmission electron microscopy (TEM) micrographs]. The PS@Au-seeds were then coated with a polyvinylpyrrolidone (PVP) layer and silanized with tetraethoxysilane, giving rise to PS@Au-seeds@SiO_2 (Figure 1a and Figure S1d−f[25]). Silica coating resulted in homogeneous shells with thicknesses of ~20 nm, as observed in high-resolution TEM (HRTEM) and scanning TEM (STEM) micrographs (Figure 2a,c). Hollow silica capsules containing Au seeds (Au-seeds@SiO_2-h; Figure 1b) were obtained by dissolving the PS cores with an ethanol/chloroform mixture (Scheme 1a, step II). Although during this step the seeds were slightly aggregated, they remained evenly distributed on the inner walls of the silica capsules. Aggregation was reflected in the UV−vis spectrum through the rise of a weak localized surface plasmon resonance (LSPR) band at 530 nm, in contrast with the featureless spectrum of the PS@Au-seeds (Figure 3a). Growth of the Au seeds inside the capsules (Au-NPs@SiO_2-h, Figure 1c) was achieved by in situ seed-catalyzed reduction of gold ions with formaldehyde (Scheme 1a, step III). Selective reduction on the surface of the seeds, even when they were embedded in the polyelectrolyte multilayer, was confirmed through control experiments, as described in Figure S2.[25]

(24) Decher, G. *Science* **1997**, *277*, 1232–1237.
(25) See the Supporting Information.

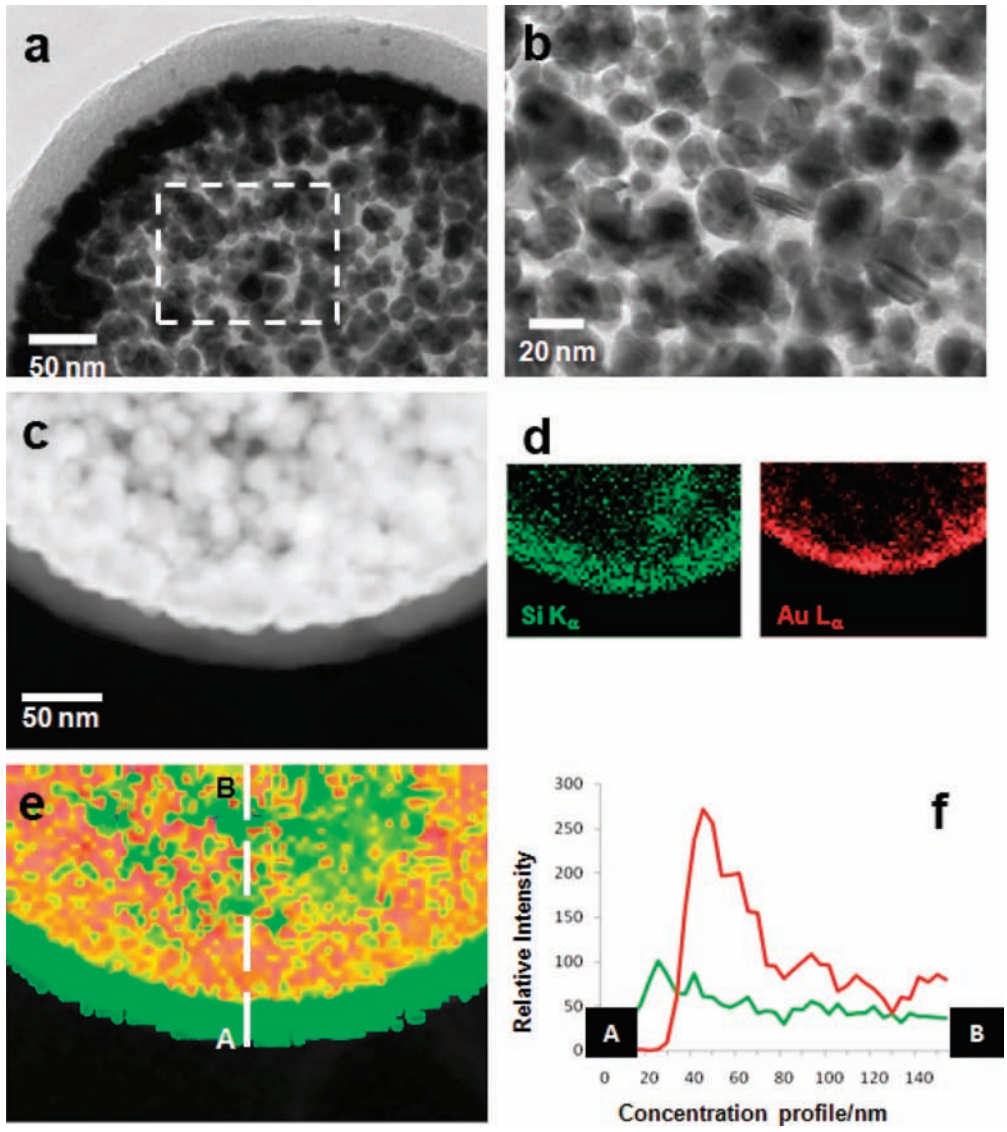

Figure 2. (a, b) HRTEM images of a Au-NPs@SiO_2-h capsule. (c) STEM image of the same capsule. (d) XEDS elemental mapping of Si and Au from the image in (c). (e) Combined XEDS mapping showing the elemental distribution. (f) XEDS profiles determined from (e) demonstrating the layered nature of the filled capsules.

Experimental Section

Unless otherwise stated, all of the chemicals were purchased from Aldrich and used without further purification.

Polystyrene Bead Functionalization and Synthesis and Adsorption of Gold Seeds (PS@Au-Seeds) (Scheme 1a, Step I). Gold seeds (1−3 nm; [Au] = 10^{-4} M) were produced as described elsewere.[26] Polystyrene bead functionalization and subsequent adsorption of gold seeds were carried out as previously reported.[16] In this case, 5 mL of functionalized PS beads (3.3 mg mL^{-1}) was added dropwise to 50 mL of a Au seed colloid and sonicated for 5 min. After 1 h, the sample was washed by three centrifugation (3000 rpm)−redispersion cycles.[27] The final concentration was 0.83 mg mL^{-1}.

Silica Coating (PS@Au-seeds@SiO_2) and Fabrication of Hollow Capsules (Au-seeds@SiO_2-h) (Scheme 1a, Step II). Silica coating was carried out following the method described by Graf et al.[28] Briefly, 400 μL of 110 mg mL^{-1} PVP (MW = 10 000) was added to 5 mL of PS@Au-seeds suspension (0.83 mg mL^{-1}). After 2 h, the suspension was washed three times by centrifugation at 3000 rpm, and the sediment was resuspended in 10 mL of a 4.2% (v/v) solution of NH_4OH in ethanol and sonicated for 5 min. Next, 43.5 μL of a 10% (v/v) solution of tetraethoxysilane (TEOS) in ethanol was added to the suspension, which was then centrifuged three times and washed with water.

Dissolution of the PS cores was carried out by shaking the bead suspension in an 1:1 ethanol/chloroform mixture in an orbital shaker for 3 days. The hollow capsules were washed and centrifuged three times, first with ethanol and then with water.

Confined Growth of Metal NPs (Au-NPs@SiO_2-h) (Scheme 1a, Step III). Au^{3+} was prereduced to Au^+ by mixing 425 μL of 0.123 M $HAuCl_4$ with 120 mL of 1.8 mM K_2CO_3 for 1 h.[27] Growth of gold seeds into nanoparticles was achieved by adding 100 mL of Au^+ solution and 300 μL of formaldehyde to 10 mL of Au-seeds@SiO_2-h under vigorous stirring. The extent of particle growth could be modulated through reaction time or amount of added Au^+. Samples were separated after 20 min of reaction

(26) Duff, D. G.; Baiker, A.; Edwards, P. P. *Langmuir* **1993**, *9*, 2301–2309.
(27) Pham, T.; Jackson, J. B.; Halas, N. J.; Lee, T. R. *Langmuir* **2002**, *18*, 4915–4920.
(28) Graf, C.; Vossen, D. L. J.; Imhof, A.; van Blaaderen, A. *Langmuir* **2003**, *19*, 6693–6700.

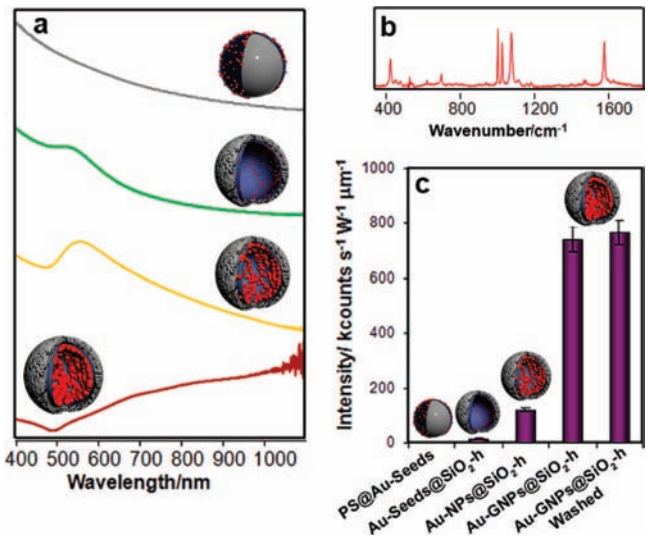

Figure 3. (a) UV−vis−NIR spectra of capsules at different growth stages, as indicated in the labels. (b) SERS spectrum of benzenethiol when excited with a 785 nm laser line. (c) Respective intensities of the ring breathing mode peaks at 999 cm^{-1} for BT adsorbed on various capsules, as indicated.

(change in color from light-pink to purple-blue) to give Au-NPs@SiO_2-h and after 18 h of reaction (purple-blue to gray-blue) to give Au-GNPs@SiO_2-h (Scheme 1a, step III). Samples were centrifuged three times and washed with water.

Characterization. TEM images were obtained using a JEOL JEM 1010 transmission electron microscope operating at an acceleration voltage of 100 kV. HRTEM, STEM, and elemental mapping by X-ray energy dispersive spectroscopy (XEDS) analysis were carried out with a JEOL JEM 2010F transmission electron microscope operating at an acceleration voltage of 200 kV. UV−vis spectra were recorded on a Cary 5000 UV−vis−NIR spectrophotometer. Spontaneous Raman scattering, SERS, and electronic emission were measured with a LabRam HR system (HORIBA Jobin Yvon) equipped with a confocal optical microscope, high-resolution gratings (1800 g mm^{-1}), and a Peltier CCD detector by using three excitation laser lines (488, 532, and 785 nm). Spectra were collected by focusing the laser line onto the sample using a 100× objective (N.A. 0.95), providing submicrometer spatial resolution, with accumulation times of 0.1−10 s. The power at the sample was varied between 10 mW and 1 μW.

Capsule Encoding (Scheme 1b, Step IV). Each of three 500 μL aliquots of the capsule suspension (0.83 mg mL^{-1}) was mixed with 100 μL of 10^{-3} M solution of an aromatic thiol [either benzenethiol (BT), 4-nitrobenzenethiol (NBT), or 4-hydroxybenzenethiol (HBT)]. After 12 h, the thiol-functionalized capsules were centrifuged (2500 rpm, 15 min) and redispersed twice. NBT-encoded particles were redispersed in ethanol to continue the functionalizion process, while BT- and HBT-codified capsules were redispersed in water. To test for possible thiol leaching, BT capsules were washed and centrifuged several times, and their SERS signals were recorded. The SERS activities of the material at different stages of the synthesis process were also monitored by using BT as probe analyte under conditions similar to those used for codification.

Biofunctionalization of Encoded Au-GNPs@SiO_2-h (Scheme 1b, Step V). Encoded capsules were primed with the silane coupling agent (3-aminopropyl)trimethoxysilane (APS) by stirring at 60−70 °C for 90 min. The amount of APS was calculated to provide the capsules with ∼1 APS molecule nm^{-2}. The capsules were then centrifuged at 2500 rpm for 15 min and washed with ethanol and phosphate-buffered saline (PBS). Carbodiimide chemistry was used to conjugate the APS primary amines with the carboxyl groups from dodecanedioic acid, providing the capsule surface with −COOH groups.[29] Briefly, 3.5 mg of dodecanedioic acid (dissolved in 0.5 mL of ethanol with 50 μL of aqueous NaOH solution) and 50 μL of 1-ethyl-3-(3-dimethylaminopropyl)-carbodiimide (EDAC) conjugation buffer [2% (w/v) EDAC, 3% (w/v) *N*-hydroxysuccinimide in PBS, pH 8.0] were mixed in an orbital shaker for 15 min at room temperature. After 2 h, the reaction was quenched with 10 μL of 1 M hydroxylamine to regenerate the original, nonreacted carboxylic groups. The carboxylic acid-conjugated capsules were centrifuged at 5000 rpm for 15 min and washed with PBS (3 × 0.5 mL). For antibody (Ab) conjugation, carbodiimide chemistry was used as in the previous step. The amount of Ab [Alexa Fluor 594 rabbit anti-goat IgG (H+L), Invitrogen] was 10 μg. When coupling was concluded, the Ab-functionalized capsules were centrifuged at 8000 rpm for 5 min and washed with PBS (3 × 0.5 mL).

Biosensing Assay (Scheme 1b, Step VI, and Scheme 1c, Steps VII and VIII). Aliquots (1.5 mL) of capsules encoded with the three different benzenethiols were centrifuged at 7300 rpm for 10 min and redispersed in 1.5 mL of the buffer [50 mM Tris, 0.14 M NaCl, 0.05% (v/v) Tween 20, pH 8.0], incubated with 10 μg of antigen (Alexa Fluor 488 goat anti-guinea pig IgG (H+L), Invitrogen) in an orbital shaker for 1 h at room temperature, and then washed and centrifuged at 7300 rpm for 10 min with water (4 × 1.5 mL) to remove unbound antigen (Scheme 1b, step VI). The capsule suspension (10 μL) was then cast onto a glass slide, air-dried, and studied within the Raman microscope with three different laser lines (785, 532 and 488 nm) (Scheme 1c, steps VII and VIII). The antigen (Ag) concentration was estimated by assuming that all of the Ab was covalently retained on the capsule surfaces during the bioimmobilization (Scheme 1b, step V).

Results and Discussion

HRTEM, STEM, and XEDS analyses (Figure 2) provide clear evidence that Au NPs grow exclusively inside the capsules, as no trace of gold was detected on the outer surfaces. This NP growth method presents clear advantages over the adsorption of NPs on PS beads or in situ adsorption and reduction of metal salts with stronger reducing agents. First, the seeds are very small, and therefore, the morphology of the hollow silica spheres is not affected. Second, and more importantly, no metal particles are present on the capsule surfaces, thereby avoiding side effects such as catalytic reactions outside the capsules or optical contamination of the SERS code. Consistent with the NP growth, Au-NPs@SiO_2-h capsules show a notable change in their optical response (Figure 3a), with enhancement and a red shift (λ_{max} = 550 nm) of the LSPR band. Gold reduction can be continued, leading to extensive growth of the NPs until they apparently fill the entire inner hollow surface (Au-GNPs@SiO_2-h, Figure 1d). In fact, the LSPR spectrum shows a dramatic absorbance increase at longer wavelengths, similar to that for gold island films, which have been demonstrated to be one of the most efficient substrates for SERS.[30]

SERS codification was achieved by immersion of the capsules into dilute solutions of selected SERS molecular probes (Scheme 1b, step IV). For the experiments reported here, the three aromatic thiols BT, NBT, and HBT were selected because they present huge SERS cross sections in the near-IR region, their vibrational spectra are clearly identifiable for each specific ring substitution (different nature and peak position), and their small sizes allow them to diffuse trough the porous silica shells[31] and be chemisorbed onto the inner gold surfaces, giving rise to very

(29) Nakajima, N.; Ikada, Y. *Bioconjugate Chem.* **1995**, *6*, 123–130.
(30) Alvarez-Puebla, R. A.; Dos Santos, D. S., Jr.; Aroca, R. F. *Analyst* **2004**, *129*, 1251–1256.
(31) van Blaaderen, A.; Vrij, A. *J. Colloid Interface Sci.* **1993**, *156*, 1–18.

stable surface complexes. The optical-enhancement properties of the particles obtained at different steps were characterized using BT as a spectroscopic probe. Figure 3b shows the SERS spectrum of BT when excited with a 785 nm laser line (spontaneous Raman spectra of the different probes are provided in Figure S3[25]). Figure 3c shows the respective intensities of the ring breathing mode peaks at 999 cm^{-1}. While the PS@Au-seeds gave no SERS signal, consistent with the absence of plasmon resonances from the small seeds (Figure 3a), upon silica coating and removal of the PS core, weak BT SERS signals were obtained as a result of partial NP aggregation. The intensity of the signal notably increased when larger particles were grown inside the capsules, ultimately leading to a dramatic enhancement when capsules with a more compact inner metal particle layer were used. This behavior is easily understood by assuming the gold-filled core to be a compact group of nanoaggregates with a large mutual interaction and LSPR coupling (a collection of hot spots). Notably, after 18 h of gold growth, no extra enhancement was achieved. Another interesting feature is the disappearance of the S−H stretching band at 2567 cm^{-1} as a consequence of the complexation of the BT thiol group to gold surface atoms (Figure S4[25]).[32] The stability of the thiol inside the capsule was confirmed by washing and centrifuging the last sample, Au-GNPs@SiO_2-h, several times with ethanol and water. Figure 3c shows that after the sample was washed, the intensity of the signal remained unchanged. We may thus conclude that the SERS label is stable and that no leaching occurs once it has been attached to the gold layer.

An additional advantage of these materials is the versatility of their surface for subsequent functionalization with the desired functional group. For the generation of surface functional groups (i.e., −COOH) that allow for the covalent conjugation of an Ab at a later stage (see the Experimental Section for details), the capsule surfaces were modified with APS. A dicarboxylic aliphatic linker was then coupled within the amino group of the outer surface, following standard carbodiimide chemistry. Carbodiimide chemistry was used as well for the immobilization of the Ab onto the modified capsules (Scheme 1b, step V). It should be noted that this process was only carried out in one of the encoded capsules, those labeled with NBT. Following the conjugation of Ab to the NBT capsules, an aliquot of the suspension of these capsules was added to equal volumes of suspensions of the capsules containing the BT and HBT codes. The resulting suspensions were sonicated for several minutes to ensure complete and homogeneous mixing. Next, 10 μg of the Ab-specific Ag was added to the capsule mixture (Scheme 1b, step VI). The suspension was subsequently washed and centrifuged in PBS and water to remove the excess Ag and then resuspended in water. A 10 μL aliquot of the capsule suspension was cast onto a glass slide, air-dried, and then studied under the confocal microscope using three different laser lines (Scheme 1c, steps VII and VIII). Figure S5[25] and Figures 4 and 5a show the spontaneous fluorescence emission spectra of the Ab [labeled with Alexa Fluor 594 (AF 594)] and the Ag [labeled with Alexa Fluor (AF 488)]. Figure 5b shows the specific SERS spectral fingerprints for the three encoded capsules.[15]

Notably, a comparison of the signals for the SERS encoding probes and the two dyes excited with the three different laser lines shows no spectroscopic contamination. Upon excititation at 785 nm, only the SERS signals are observed, in agreement with Figure 4a. The molecular absorptions are completely out of resonance with the infrared laser; thus, no molecular emission is observed. Excitation with the green laser (532 nm) yields no SERS signal but does produce strong and weak emission of

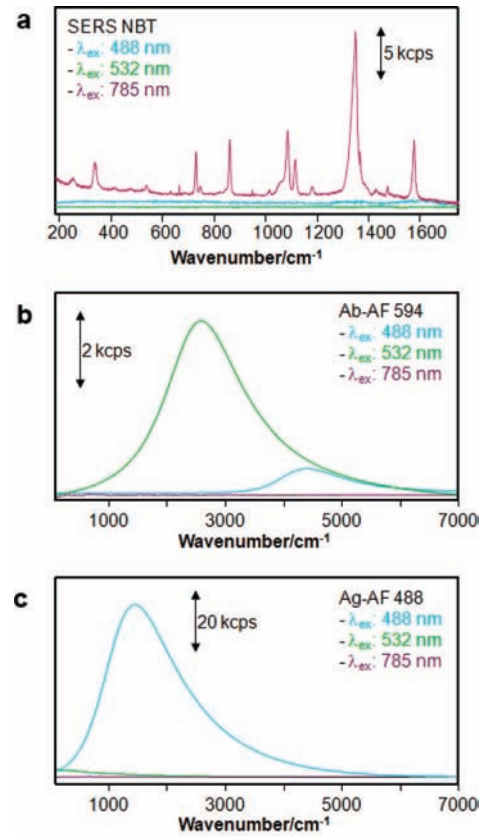

Figure 4. Comparison of the signals for the SERS encoding probes and the two dyes excited with three different laser lines.

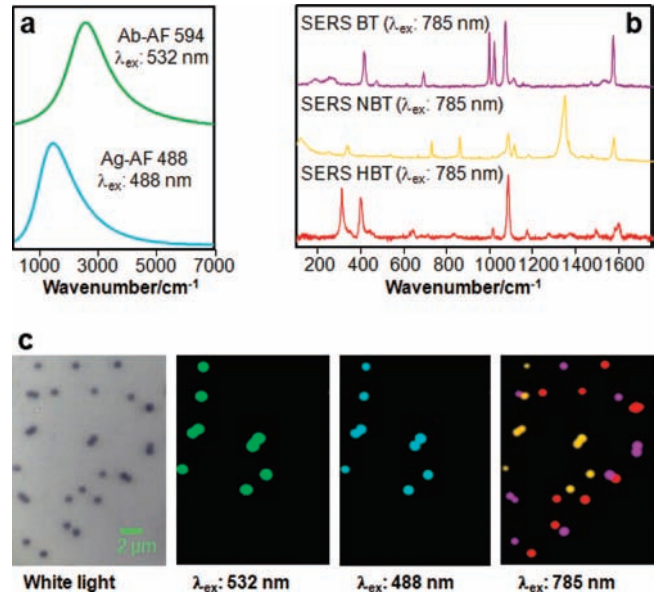

Figure 5. (a) Fluorescence emission spectra of AF 594 and AF 488, bound to the Ab and Ag, respectively. (b) SERS spectra of BT, NBT, and HBT (as labeled) upon excitation with a 785 nm laser line. (c) Images from a small area of the substrate with a random distribution of encoded capsules. The leftmost image is an optical micrograph, while the other three are SERS mappings obtained by illumination with the three different laser lines, as indicated.

(32) Joo, T. H.; Kim, K.; Kim, M. S. *J. Raman Spectrosc.* **1987**, *18*, 57–60.

AF 594 and AF 488, respectively (Figure 4b). For Au nanoparticles with a plasmon peak located at ~520 nm or higher energies, the SERS signal is extremely weak or undetectable. This is mainly a result of the fact that the interband transitions severely depress the LSPR. The strong SERS signal can be obtained from Au NPs only for excitation wavelengths longer than 600 nm. The green laser is in resonance and preresonance with AF 594 and AF 488, respectively. Excitation with the blue laser (488 nm) gives rise to strong emission from AF 488 (in resonance), very weak emission from AF 594 (out of resonance), and no SERS (excitation is blue-shifted with respect to the plasmon) (Figure 4c).

Figure 5c is a clear demonstration of the encoding capabilities of these particles. All of the images were obtained from the same area of the substrate, which contained a random distribution of spheres, as shown in the white-light image. Upon illumination with the 532 nm laser line, only the particles where the Ab was anchored were imaged (the fluorescence of AF 594 was excited), while upon illumination with the 488 nm laser line, the very same particles were observed, indicating the successful Ab−Ag biocoupling (AF 488 was selectively excited). Notably, the absence of a fluorescence background for the other codified particles demonstrates that the Ag was not retained in the absence of the coupling agent. Finally, when the SERS signal was measured over the same area under 785 nm illumination, deconvolution of all of the encoded capsules was achieved. It should be noted that all of the yellow capsules (corresponding to particles codified with NBT) perfectly fit with both fluorescence maps, demonstrating an accurate identification of the active particles with no signal of cross-reactivity even at such a small scale. The time required for complete analysis and deconvolution of the images was less than 1 min, which clearly shows the high potential of this system for multiplexing and high-throughput biomedical screening applications.

Conclusions

In summary, these results demonstrate the efficiency of antibody conjugation and on-particle antigen recognition at a very low content ($<2 \times 10^{-9}$ mg, as estimated from the illuminated cross section of a single particle under the assumption that all of the Ab was covalently retained on the capsule surfaces) within short acquisition times (less than 1 s per particle) and with an unprecedented submicrometer spatial resolution, providing an excellent material for high-throughput screening. Furthermore, the readiness of the capsule surfaces to be functionalized with the desired functional group increases the scope of application to the design and solid-phase synthesis of combinatorial libraries for drug discovery,[33] either when mounted onto patterned substrates or in real time using Raman flow cytometry.[34] Additionally, many potential uses can be envisioned for the as-prepared submicroreactors with active metallic nanoparticles inside, such as local overheating inside the reactor without affecting the solvent outside the particles. Moreover, this ability for confined growth of inorganic species provides a unique strategy for the synthesis of complex nanostructures with accurate size and shape control.

Acknowledgment. This work was supported by the Spanish MEC (MAT2007-62696; MAT2008-05755/MAT; Consolider-Ingenio Nanobiomed) and Xunta de Galicia (PGIDIT06TMT31402PR; PGIDIT03TMT30101PR). M.A.C.-D. and R.A.Á.-P. acknowledge financial support from the *Isidro Parga Pondal* Program (Xunta de Galicia, Spain) and the *Ramon y Cajal* Program (Ministerio de Educación y Ciencia, Spain).

Supporting Information Available: TEM images and Raman, SERS, and fluorescence spectra. This material is available free of charge via the Internet at http://pubs.acs.org.

JA8088444

(33) Fenniri, H.; Ding, L.; Ribbe, A. E.; Zyrianov, Y. *J. Am. Chem. Soc.* **2001**, *123*, 8151–8152.
(34) Watson, D. A.; Brown, L. O.; Gaskill, D. F.; Naivar, M.; Graves, S. W.; Doorn, S. K.; Nolan, J. P. *Cytometry* **2008**, *73A*, 119–128.